

Calcium Valence-to-Core X-ray Emission Spectroscopy: A Sensitive Probe of Oxo Protonation in Structural Models of the Oxygen-Evolving Complex

Supporting Information

Zachary Mathe,[†] Dimitrios A. Pantazis,[‡] Heui Beom Lee,[§] Richard Gnewkow,^{||}
Benjamin E. Van Kuiken,[†] Theodor Agapie,[§] Serena DeBeer^{*,†}

[†]Max-Planck-Institut für Chemische Energiekonversion, Stiftstrasse 34-36, D-45470 Mülheim an der Ruhr, Germany

[‡]Max-Planck-Institut für Kohlenforschung, Kaiser-Wilhelm-Platz 1, D-45470 Mülheim an der Ruhr, Germany

[§]Division of Chemistry and Chemical Engineering, California Institute of Technology, Pasadena, California 91125, United States

^{||}Technical University of Berlin, Institute of Optics and Atomic Physics, Hardenbergstraße 36, D-10587 Berlin, Germany.

S1.	<i>Further Computational Details</i>	2
S2.	<i>Crystal Structures of Calcium Salts</i>	3
S3.	<i>Kβ Mainline Transitions</i>	4
S4.	<i>Multiply Excited States and CaF₂</i>	5
S5.	<i>Calcium 1s Orbital Energies</i>	6
S6.	<i>CaCO₃ Molecular Orbitals</i>	7
S7.	<i>Löwdin Population Analysis of Molecular Complexes</i>	8
S8.	<i>Insensitivity of 1H Spectra to the Triflate Counterion</i>	10
S9.	<i>Instrument Response Function and Resolution</i>	11
S10.	<i>References</i>	12

S1. Further Computational Details

Ca(OH)₂ Crystal Structure

In Ca(OH)₂, all calcium and oxygen sites are equivalent, but a neutron diffraction study revealed three distinct proton sites at both 80 and 293 K.¹ The sites are equidistant from the corresponding oxygen atom, and the experiment was unable to resolve whether their equal occupations are static or in dynamic equilibrium. Embedding models were constructed from a modified crystal structure with the protons in the average position of the three true sites.

Uniform Absolute Energy Shift

Though the computational protocol used here provides accurate relative energies in the valence region, the absolute energies of core orbitals, and hence valence-to-core transitions, are systematically inaccurate due to limitations of the one-particle basis sets and density functionals near the nucleus.² The energy correction required to obtain agreement with experiment depends on the element, functional and basis set. Here, a shift of +71.1 eV was found by least-squares linear regression of calculated versus experimental VtC peak energies, constrained to include the origin (Figure S1). Peak energies were determined for this and all other purposes by taking the maximum of an asymmetric pseudo-Voigt function fitted to the top ~10% of the apparent peak.

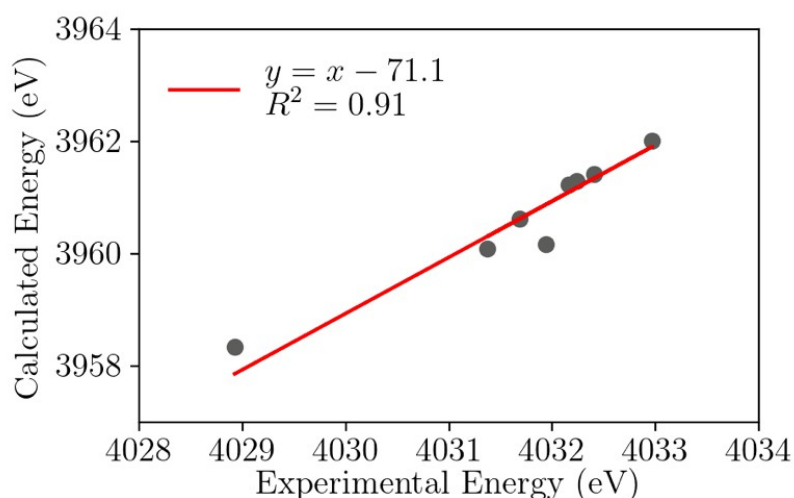


Figure S1. Linear regression to obtain the absolute energy shift for DFT-calculated transition energies. The molecular complex **2** was excluded from this calibration as it lacked a well-defined VtC maximum. CaI₂ was excluded because it was calculated with a different basis set.

S2. Crystal Structures of Calcium Salts

Approximate symmetries and bond lengths of the calcium sites in the seven salts are presented in Table 1 of the main text. Renderings of the calcium sites, all at the same scale, are presented in Figure S2.

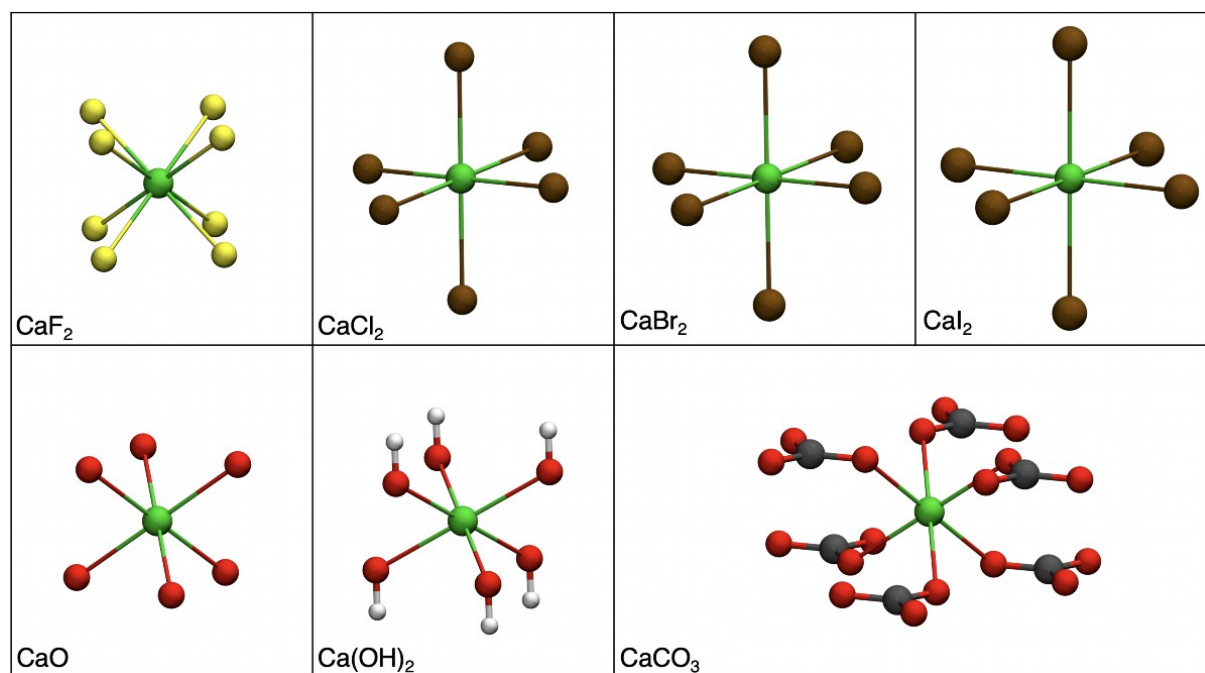


Figure S2. Renderings of the seven calcium salts, all at the same scale.

S3. $K\beta$ Mainline Transitions

We have referred to the $K\beta_{1,3}$ and $K\beta''$ features of a calcium $K\beta$ XES spectrum collectively as the $K\beta$ mainline because these features are so close in energy that the $K\beta''$ is observed either as a small shoulder to the $K\beta_{1,3}$ peak or not at all. In the MO framework, this means that the highest-energy ligand s orbitals are close in energy to the calcium 3p orbitals. $K\beta''$ peaks can be distinguished in certain cases. Figure S3 presents mainline spectra for CaO and Ca(OH)₂. The mainline in Ca(OH)₂ appears as a single broad peak, while in CaO there is a clear shoulder at 4016 eV. The calculations reveal that the difference is due to the energies of the underlying $K\beta''$ peaks. Compared to those of CaO, the oxygen 2s orbitals of Ca(OH)₂ are stabilized by the nearby protons, shifting the emission energy 2 eV closer to the $K\beta_{1,3}$.

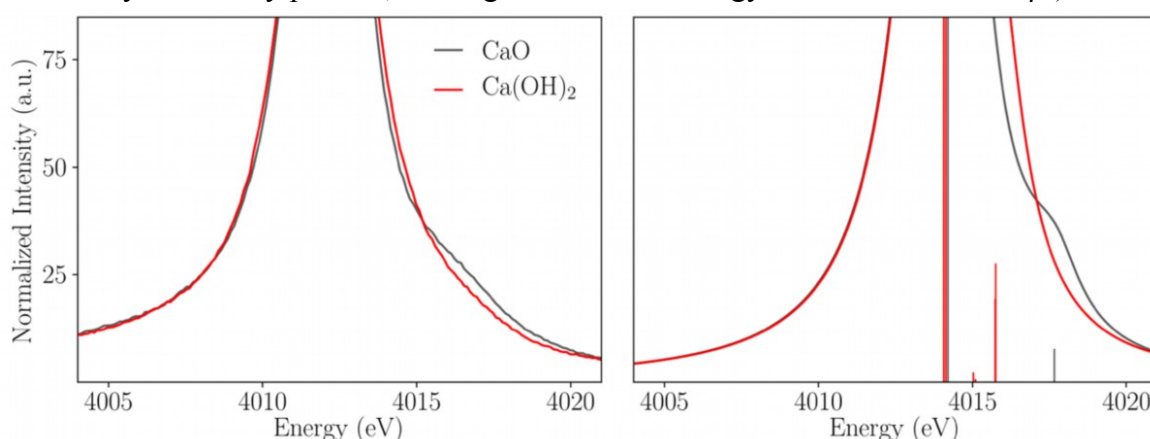


Figure S3. Observed (left) and calculated (right) $K\beta$ mainlines of CaO and Ca(OH)₂, including individual calculated transitions as sticks.

Another comparison is found between CaF₂ and CaCl₂ (Figure S4). The small shoulder at 4008 eV in the CaF₂ spectrum is a $K\beta''$ transition from a fluorine 2s orbital, to our knowledge the first case of a $K\beta$ VtC transition at a lower energy than the metal mainline. In CaCl₂, the corresponding transition is calculated at 4021 eV. Due to the low intensity of $K\beta''$ features, the degrees of freedom introduced by the spectrometer's asymmetric response function and the possible presence of multiply excited intermediate states (vide infra), curve fitting of the mainline to extract $K\beta''$ data was not pursued. With a higher-resolution instrument or precise knowledge of the instrument response function, calcium $K\beta''$ features might have diagnostic utility.

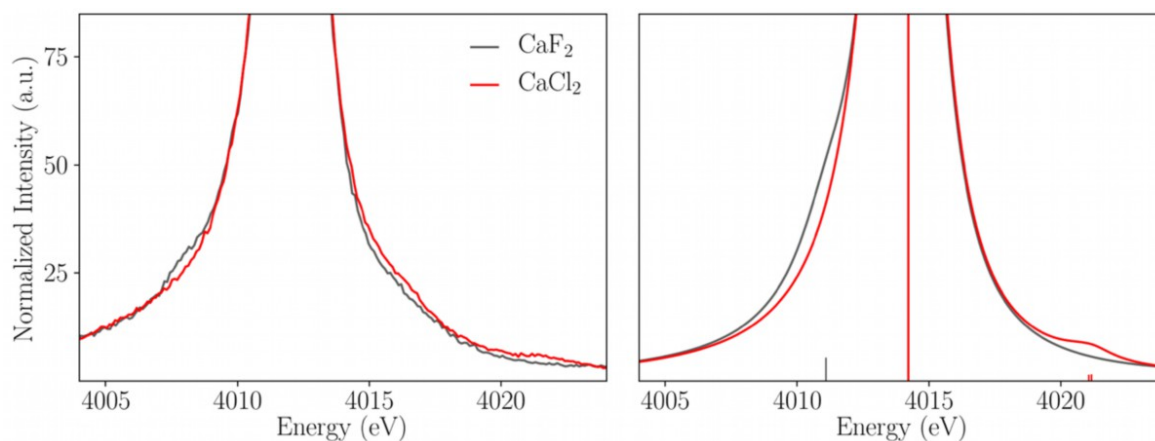


Figure S4. Observed (left) and calculated (right) $K\beta$ mainlines of CaF₂ and CaCl₂, including individual calculated transitions as sticks.

S4. Multiply Excited States and CaF₂

In addition to the diagram lines discussed in the main text (emission events from an excited intermediate state with a 1s hole), K β emission spectra may contain features due to transitions from multiply excited intermediate states generated via shake-up (SU) and shake-off (SO) processes.³⁻⁵ Electron SU and SO occur when the production of a 1s hole is accompanied by the excitation of a second electron to a higher bound state or the continuum, respectively. Emission from multiply excited states is not typically considered in bioinorganic X-ray spectroscopy, partly because the interpretive frameworks appropriate for the analysis of molecular coordination environments are not applicable to such transitions.

In a 2018 study,⁴ Ito and coworkers performed high-resolution K β emission measurements for elements from calcium to germanium. To our knowledge, this publication includes the only prior reported analysis of calcium K β emission. Transitions, including those from SU and SO multiply excited intermediate states, were calculated using a multiconfigurational Dirac-Fock (MCDF) method that is well-established for such atomic physical investigations. The calcium MCDF calculations were performed from a Ca⁰ electron configuration, [Ne]3s²3p⁶4s², and calculated spectra included significant intensity from [1s4s] double-hole excited states. However, the spectroscopy was performed with a sample of CaF₂. Calcium in CaF₂ (and most all stable calcium compounds) has an oxidation state of 2+ and an empty 4s shell.^{6,7} Thus, the computational approach was not suitable for modeling the approximately-atomic features in the experimental data. It is also clear from the present investigation that inclusion of VtC transitions, which were entirely neglected, is essential to understanding Ca K β mainlines.

In Ito 2018, the low-energy shoulder of the CaF₂ mainline is labeled K β' . The authors write that, “we may conclude that the K β' and K β'' peaks result mainly from the [KM] shake process, proving that these peaks do not correspond to diagram lines.” ([KM] shake processes refer to the generation of intermediate states with both a 1s hole and a 3s or 3p hole.) This same feature is assigned here (vida supra) to a diagram line, namely a K β'' VtC transition from a Ca 1s hole intermediate state to a fluorine 2s hole final state. As this feature varies significantly between CaF₂ and CaCl₂, it cannot be considered approximately atomic. In the view of the present authors, though a VtC transition is the more plausible assignment, future investigations of K β XES could benefit from a combined DFT and MDCF analysis.

S5. Calcium 1s Orbital Energies

Spectra for a series of hypothetical CaCl_2 crystals with varying average Ca–Cl distances were presented in the main text, showing a linear correlation between distance and $\text{K}\beta_{2,5}$ peak energy. This trend is due to additive trends of similar magnitude in the donor and acceptor orbital energies: as the Ca–Cl distance increases, the Cl 3p energy increases and the Ca 1s energy decreases (Figure S5). Both of these effects can be rationalized with simple electrostatic arguments. Cl 3p orbitals are stabilized by the proximity of positively-charged calcium cations, while Ca 1s orbitals are destabilized by nearby chloride anions. This explanation is supported by calculations performed with point charges replacing one ion type, which show effects of similar magnitude.

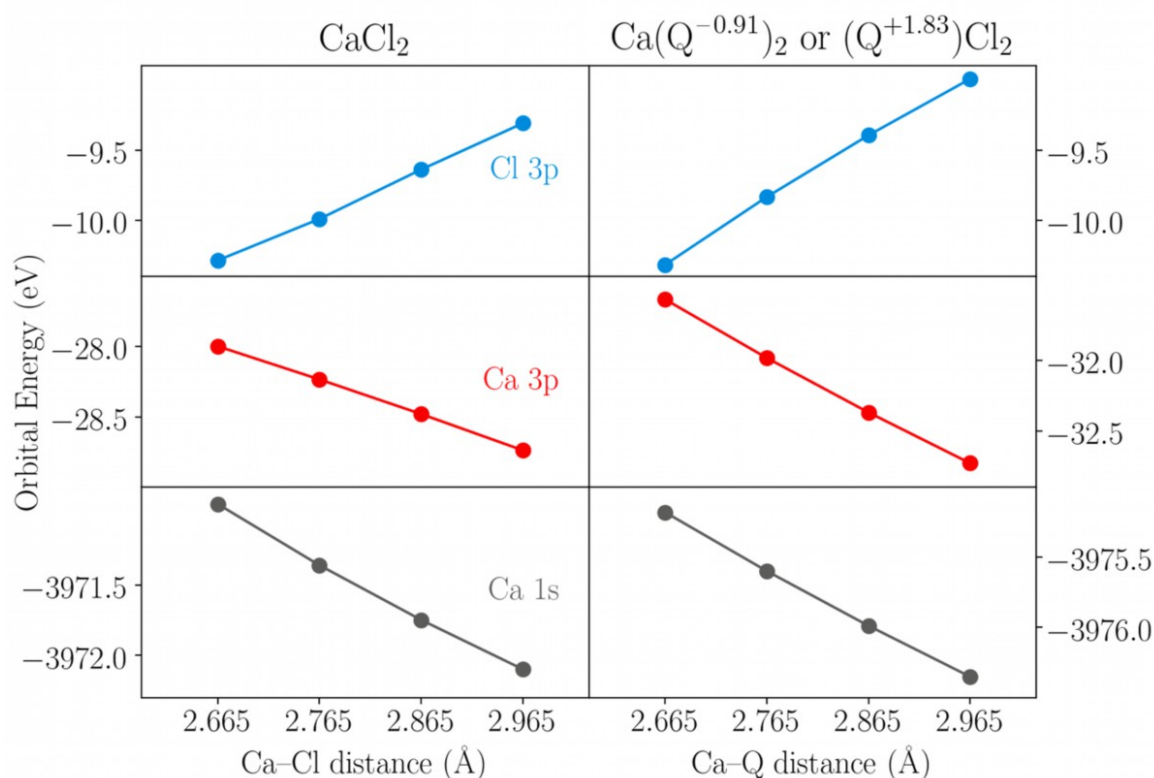


Figure S5. Orbital energies of the Ca 1s (grey), Ca 3p (red), and Cl 3p (blue) orbitals as a function of Ca–Cl distance. In the left column, the usual embedding procedure was used, while in the right column, all Ca or Cl atoms were replaced with point charges. In each model, the orbital with the most intense $\text{K}\beta_{2,5}$ emission was chosen. Each plot spans 1.5 eV on the vertical axis.

S6. CaCO₃ Molecular Orbitals

Plots of representative orbitals from the four transition regions of CaCO₃ are presented in Figure S6.

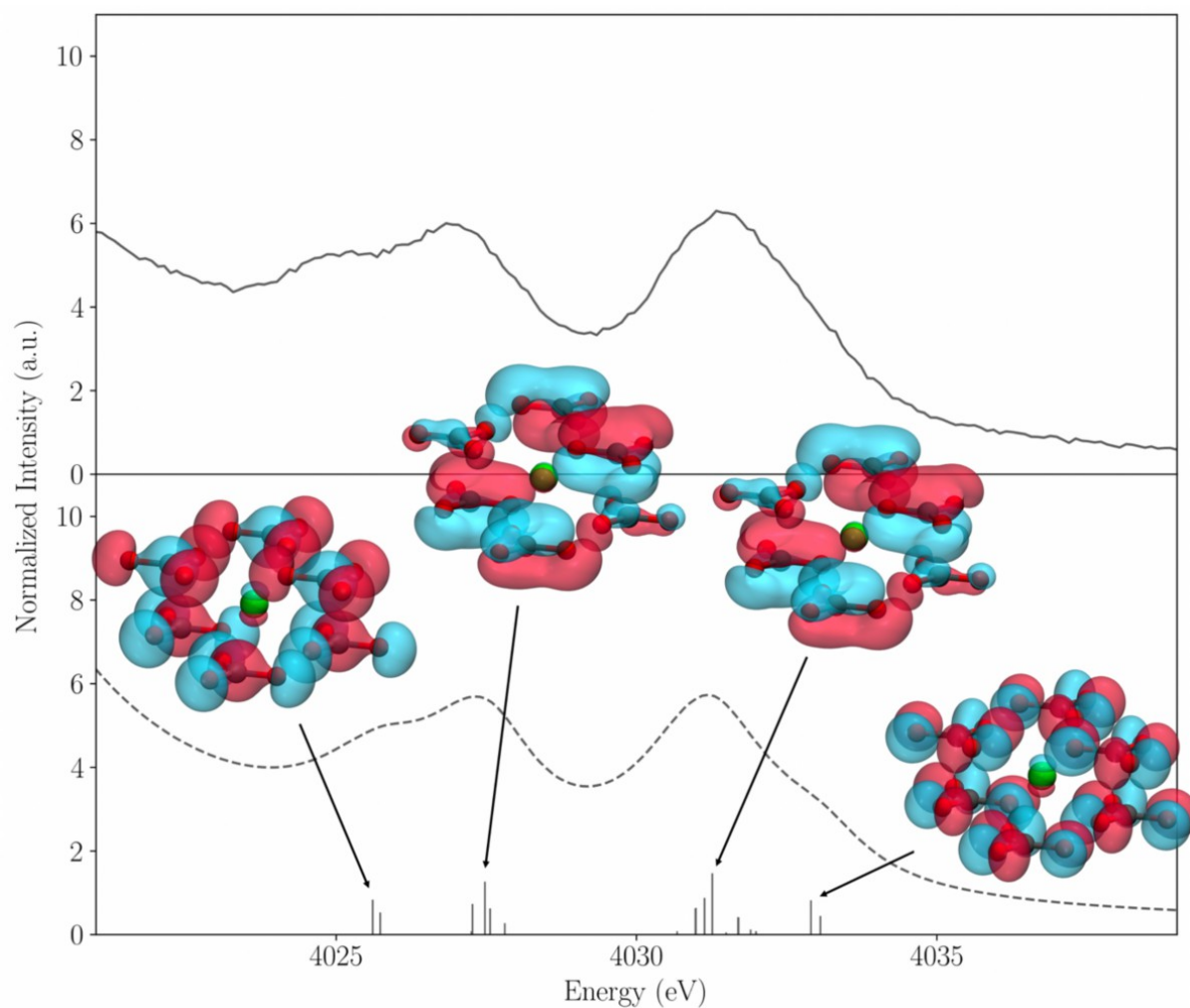


Figure S6. Observed and calculated $K\beta_{2.5}$ spectra of CaCO₃ (solid and dashed lines), with plots of representative orbitals from each of the four groups of transitions with isovalues of ± 0.02

S7. Löwdin Population Analysis of Molecular Complexes

It is a common practice in X-ray spectroscopy to assign the character of donor (or acceptor) orbitals using Löwdin population analysis, a method of expressing the basis function contributions to each MO.^{2,8-12} In small, highly-symmetric systems, such analysis is useful in assigning spectral features and extracting chemical insight. However, the interpretation of Löwdin populations in chemically-familiar terms relies on the assumption that each basis function, centered on a particular atom and with a particular angular momentum, makes an atomic-orbital-like contribution to the total wave function. This is not always the case: basis functions centered on one atom can be used to describe the electronic structure associated with a different atom (as in basis set superposition error), and basis functions with higher angular momenta are used to polarize MOs with lower angular momenta. Thus, it is not necessarily sensible to interpret Löwdin populations as indicators of e.g. the *calcium character* or *p character*, at least in the sense familiar to many chemists.

Moreover, when calculating transitions involving a delocalized valence MO, there may arise another problem. Canonical MOs do not necessarily express any information about the bonding, interactions or correlation between different moieties; they are constructed only to have well-defined energies. Thus, in a large molecule, a canonical MO may contain contributions from basis functions with distant centers. Figure S7 shows plots of two intense $K\beta_{2,5}$ donor MOs for complex **1**, 318 β and 352 β . MO 318 β has large cubane oxygen p lobes and aromatic lobes on one of the L pyridyl groups, as well as some smaller contributions. MO 352 β is more delocalized, with contributions localized to pyridyl, benzyl and alkoxy groups on L, to oximate and amine groups on ON₄O, and to the cubane.

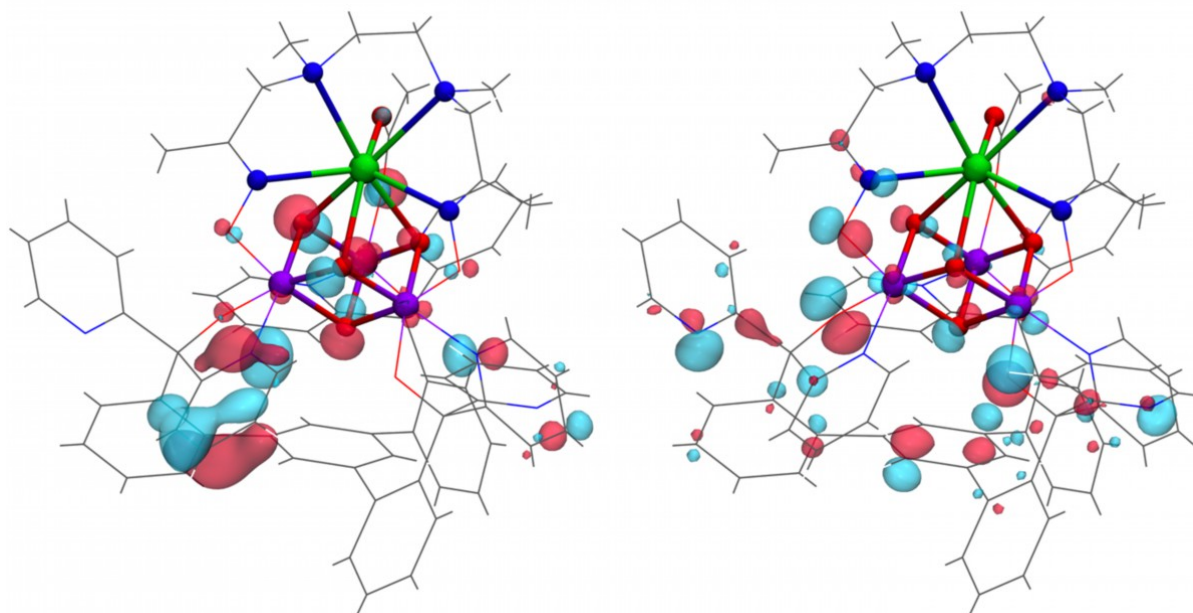


Figure S7. Plots of MOs 318 β and 352 β for complex **1**. They are donor orbitals for two of the most intense 15% of transitions in the $K\beta_{2,5}$ region.

With these facts about MOs in mind, we present spectra calculated from transitions with intensities scaled by the contributions to the donor MO from different moieties, determined by

Löwdin population (Figure S8). If one had not considered the above discussion, one might conclude that the ligand L is the most important contributor to calcium VtC emission, as its Löwdin-scaled spectrum defines both the overall spectral envelope and the differences between **1** and **1H**. However, Figure S8 actually reflects the fact that most of the donor MOs are highly delocalized, and the large ligand L contains most of the total basis functions. To verify this interpretation, spectra were calculated for **1noL** and **1HnoL**, truncated structures of **1** and **1H** constructed by replacing L with $-OH$ and $-NH_3$ groups and reoptimizing only hydrogen atoms (Figure S9). The total spectra are similar to those of the full complexes, while the Löwdin contributions of the cubane and the ON_4O ligand change dramatically. Thus, we must conclude that Löwdin population analysis is not an optimal tool for analyzing spectra of these systems, and may be vulnerable to misinterpretation.

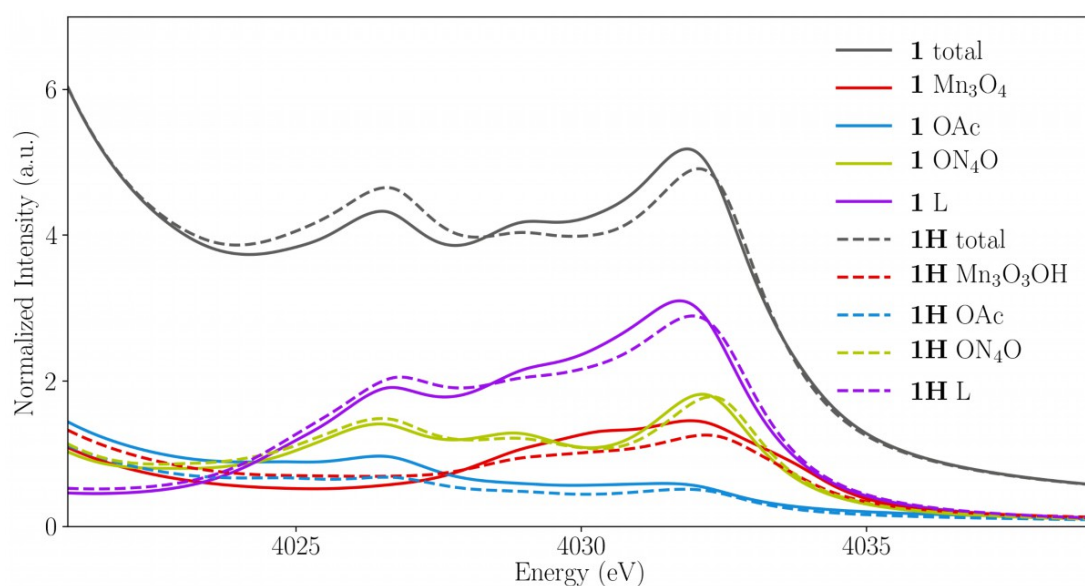


Figure S8. Calculated spectra of **1** and **1H**, together with spectra scaled by the contributions from different moieties as determined by Löwdin population. The scaled spectra have been multiplied by 1.5 to reduce clutter.

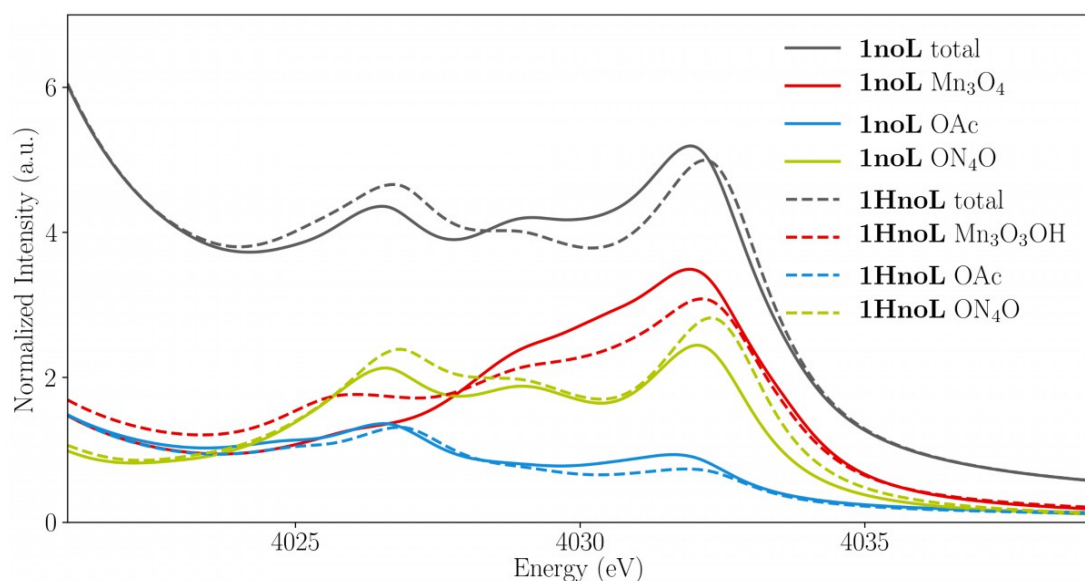


Figure S9. Calculated spectra of **1noL** and **1HnoL**, together with spectra scaled by the contributions from different moieties as determined by Löwdin population. The scaled spectra have been multiplied by 1.5 to reduce clutter.

S8. Insensitivity of **1H** Spectra to the Triflate Counterion

The triflate counterion was included in calculations of **1H** due to its proximity to the calcium and cubane hydroxo (Figure S10). With the triflate omitted, the optimized geometry had worse agreement with crystallographic bond lengths. However, the calculated Ca VtC spectra of **1H** were equivalent, regardless of the presence of the triflate in the geometry optimization or final single-point calculation, demonstrating that it did not contribute significantly to the VtC XES spectra (Figure S11).

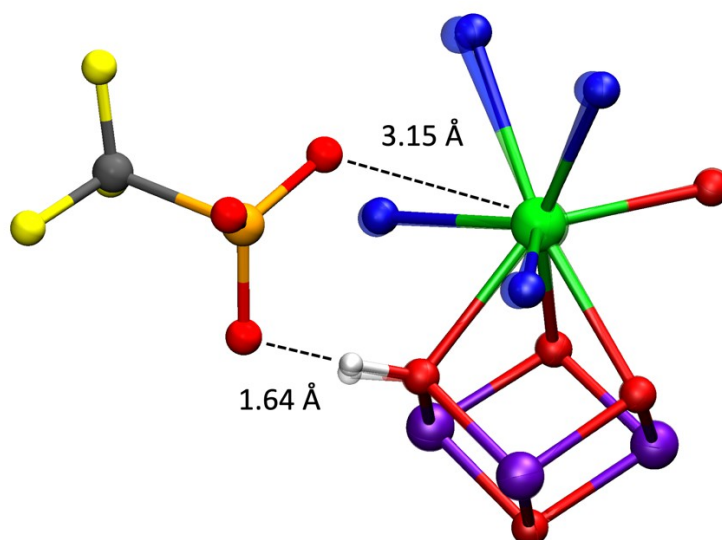


Figure S10. Structure of **1H** showing the triflate counterion (opaque), plus a structure re-optimized without the triflate (translucent)

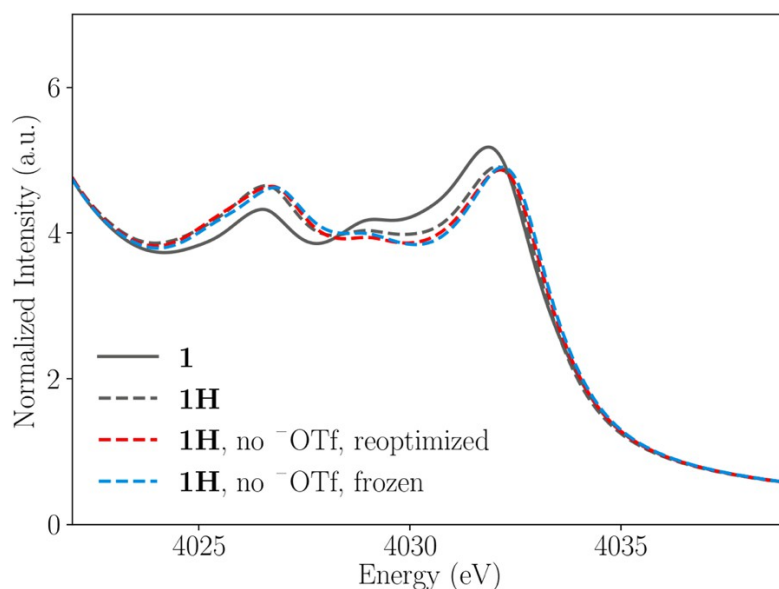


Figure S11. Spectra of **1** and **1H**, including the full structure of **1H** (grey), the structure re-optimized without the triflate (red), and the coordinates from the full structure with the triflate removed (blue).

S9. Instrument Response Function and Resolution

The spectrum S observed in a photon emission experiment can be expressed as the convolution of functions $S = N * R$, where N is the spectrum actually emitted by the sample, determined by the underlying physical process, and R is the instrument response function to an ideal zero-width signal, determined by the spectrometer optics and detector. X-ray emission in the solid phase is dominated by lifetime broadening, resulting in an N that is a sum of symmetric Lorentzian functions. While most spectrometers have symmetric Gaussian response functions, the LabXES spectrometer has an asymmetric Voigt response due to the mosaic structure of the highly annealed pyrolytic graphite (HAPG) Bragg optic.^{13,14} This material was used despite the suboptimal response function because it allows the construction of a full-cylinder optic and has higher integral reflectivity than an ideal optic, thus maximizing the effective solid angle of detection and hence signal strength. The theoretical spectra presented in this investigation were calculated from DFT transitions using an asymmetric pseudo-Voigt function with parameters chosen to approximate the observed LabXES spectra.

Figure S12 presents OEC S_1 state spectra calculated with the approximate LabXES response function, as well as with a higher-resolution symmetric response function. The latter spectrum approximates that which could be obtained using a modern synchrotron spectrometer equipped with a traditional crystal Bragg optic.

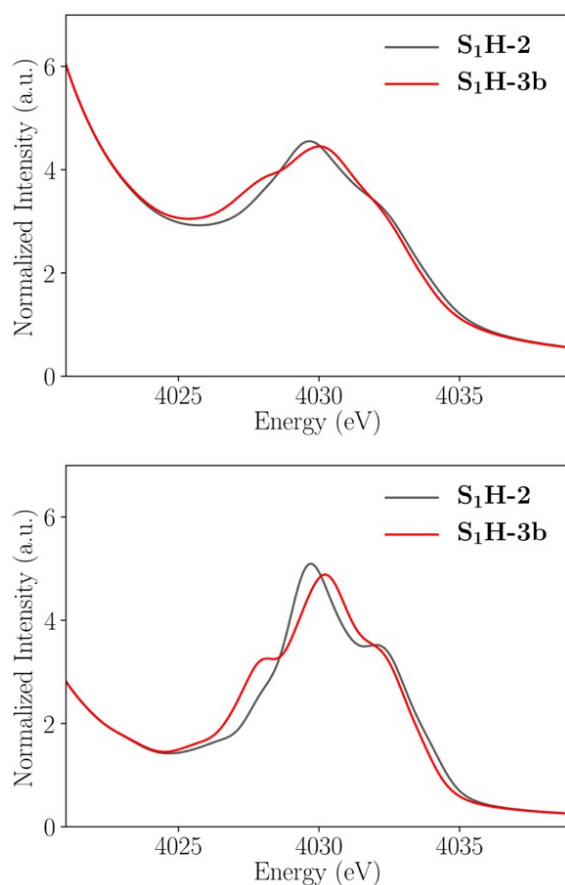


Figure S12. Calculated spectra for two computational models of the S_1 state of the OEC, demonstrating the improved resolution that might be obtained using a synchrotron-based dispersive spectrometer.

S10. References

- (1) Desgranges, L.; Grebille, D.; Calvarin, G.; Chevrier, G.; Floquet, N.; Niepce, J. -C. Hydrogen Thermal Motion in Calcium Hydroxide: Ca(OH)₂. *Acta Crystallogr. Sect. B* **1993**, *49*, 812–817.
- (2) Pollock, C. J.; DeBeer, S. Insights into the Geometric and Electronic Structure of Transition Metal Centers from Valence-to-Core X-Ray Emission Spectroscopy. *Acc. Chem. Res.* **2015**, *48*, 2967–2975.
- (3) Glatzel, P. Multiple Excitations in the K Fluorescence Emission of Mn, Fe and Ni Compounds. *AIP Conf. Proc.* **2003**, *652*, 250–255.
- (4) Ito, Y.; Tochio, T.; Yamashita, M.; Fukushima, S.; Vlaicu, A. M.; Syrocki; Słabkowska, K.; Weder, E.; Polasik, M.; Sawicka, K.; Indelicato, P.; Marques, J. P.; Sampaio, J. M.; Guerra, M.; Santos, J. P.; Parente, F. Structure of High-Resolution K $\beta_{1,3}$ X-Ray Emission Spectra for the Elements from Ca to Ge. *Phys. Rev. A* **2018**, *97*, 1–10.
- (5) Carlson, T. A.; Nestor, C. W. Calculation of Electron Shake-off Probabilities as the Result of X-Ray Photoionization of the Rare Gases. *Phys. Rev. A* **1973**, *8*, 2887–2894.
- (6) Speziale, S.; Duffy, T. S. Single-Crystal Elastic Constants of Fluorite (CaF₂) to 9.3 GPa. *Phys. Chem. Miner.* **2002**, *29*, 465–472.
- (7) Hill, M. S.; Liptrot, D. J.; Weetman, C. Alkaline Earths as Main Group Reagents in Molecular Catalysis. *Chem. Soc. Rev.* **2016**, *45*, 972–988.
- (8) Pollock, C. J.; DeBeer, S. Valence-to-Core X-Ray Emission Spectroscopy: A Sensitive Probe of the Nature of a Bound Ligand. *J. Am. Chem. Soc.* **2011**, *133*, 5594–5601.
- (9) Beckwith, M. A.; Roemelt, M.; Collomb, M.-N.; DuBoc, C.; Weng, T.-C.; Bergmann, U.; Glatzel, P.; Neese, F.; DeBeer, S. Manganese K β X-Ray Emission Spectroscopy As a Probe of Metal–Ligand Interactions. *Inorg. Chem.* **2011**, *50*, 8397–8409.
- (10) Rees, J. A.; Martin-Diaconescu, V.; Kovacs, J. A.; DeBeer, S. X-Ray Absorption and Emission Study of Dioxygen Activation by a Small-Molecule Manganese Complex. *Inorg. Chem.* **2015**, *54*, 6410–6422.
- (11) Delgado-Jaime, M. U.; DeBeer, S.; Bauer, M. Valence-to-Core X-Ray Emission Spectroscopy of Iron-Carbonyl Complexes: Implications for the Examination of Catalytic Intermediates. *Chem. - A Eur. J.* **2013**, *19*, 15888–15897.
- (12) Lee, N.; Petrenko, T.; Bergmann, U.; Neese, F.; DeBeer, S. Probing Valence Orbital Composition with Iron K-Beta X-Ray Emission Spectroscopy. *J. Am. Chem. Soc.* **2010**, *132*, 9715–9727.
- (13) Malzer, W.; Grötzsch, D.; Gnewkow, R.; Schlesiger, C.; Kowalewski, F.; Van Kuiken, B.; DeBeer, S.; Kanngießner, B. A Laboratory Spectrometer for High Throughput X-Ray Emission Spectroscopy in Catalysis Research. *Rev. Sci. Instrum.* **2018**, *89*, 113111.
- (14) Anklamm, L.; Schlesiger, C.; Malzer, W.; Grotzsch, D.; Neitzel, M.; Kanngiesser, B. A Novel von Hamos Spectrometer for Efficient X-Ray Emission Spectroscopy in the Laboratory. *Rev. Sci. Instrum.* **2014**, *85*.